



Article

Difference in Surface Damage between Deep and Shallow Mining of Underground Coal Resources in China

Weitao Yan ^{1,2}, Junting Guo ^{1,*} and Shaoge Yan ²

¹ State Key Laboratory of Groundwater Protection and Utilization by Coal Mining, Beijing 102009, China; yanweitao@hpu.edu.cn

² State Collaborative Innovation Center of Coal Work Safety and Clean-Efficiency Utilization, Henan Polytechnic University, Jiaozuo 454003, China; yanshaoge@hpu.edu.cn

* Correspondence: guojunting@nicenergy.com

Abstract: The mining of underground coal resources often results in extensive damage to the ground surface, particularly in China, which has a large amount of coal resources. However, the laws of surface damage caused by the mining of deep and shallow underground coal resources are relatively different. This study analyzes the difference in surface damage induced by deep and shallow mining and its mechanism by field measurement and similar material simulation experiments. Surface damage is mainly manifested in the form of cracks, which can be categorized as permanent and dynamic cracks. Permanent cracks occur above the mining boundary of shallow and deep coal mines. Dynamic cracks (including dynamic stretching cracks and stepped cracks) only appear above the goaf in shallow mining. This disparity is due to the fact that strata movement in deep mining occurs in a “three zones” mode, with the failure height of strata increasing with the mining degree in an “S” shape. However, rock strata movement in shallow mining follows a “two zones” mode, with the failure height of rock strata increasing exponentially with the mining degree. Thus, the rock strata are prone to slide and become unstable in the form of benched rock beams, producing dynamic cracks, such as stepped cracks on the surface. This research improves the existing mining subsidence theory and provides technical support for relevant mines to take targeted treatment measures.



Citation: Yan, W.; Guo, J.; Yan, S. Difference in Surface Damage between Deep and Shallow Mining of Underground Coal Resources in China. *Sustainability* **2023**, *15*, 7296. <https://doi.org/10.3390/su15097296>

Academic Editor: Baoqing Li

Received: 13 March 2023

Revised: 21 April 2023

Accepted: 24 April 2023

Published: 27 April 2023



Copyright: © 2023 by the authors. Licensee MDPI, Basel, Switzerland. This article is an open access article distributed under the terms and conditions of the Creative Commons Attribution (CC BY) license (<https://creativecommons.org/licenses/by/4.0/>).

1. Introduction

China has the largest coal production in the world, with a production of 4.5 billion tons in 2022, accounting for 54% of the world's total output [1]. The extraction of a large amount of underground coal resources leads to a large range of surface damage, including surface water accumulation [2], cracks [3,4], underground pipeline damage, and vegetation damage [5,6]. It has a serious impact on the local environment and undermines the sustainable development of the local economy, society, and ecology (Figure 1).

Coal seams can be classified into shallow, middle-deep, and deep, based on their depth and relevant mining science knowledge. A coal seam buried more than 400 m deep is considered a deep coal seam, a coal seam buried less than 200 m deep is a shallow coal seam, and a coal seam buried between 200 and 400 m deep is a middle-deep coal seam (Figure 1) [7,8].

Mining of underground coal seams with different burial depths results in varying degrees of surface damage. The impact of underground mining spreads through the overburden and ultimately affects the surface, causing surface damage [9]. The deeper the coal seam is buried, the longer the transmission path required for the mining impact to spread to the surface, and the greater the mining impact reduction, the greater the surface damage range, and the smaller the surface damage degree [10].

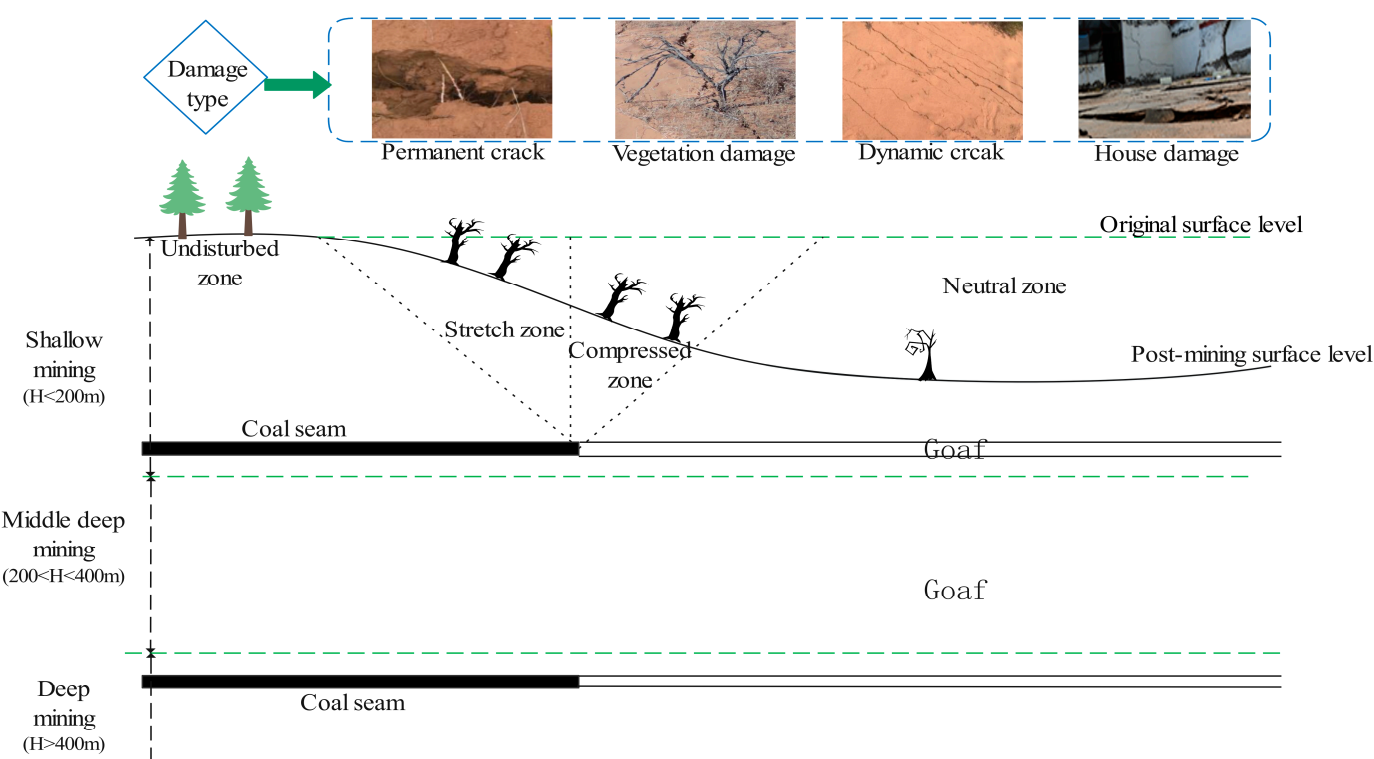


Figure 1. Surface damage induced by mining.

At present, many scholars have conducted extensive research on shallow and deep mining, leading to various research results. Scholars have integrated a variety of monitoring technologies to conduct multisource, integrated surface damage monitoring [11–15]. The law of mining surface damage is clarified on the basis of multisource fusion data [16,17]. The damage mechanism of overburden and surface is revealed by various means [18–21], and the prediction model of surface subsidence is built by combining various algorithms [22–25].

However, most of the results only analyze the surface damage caused by either shallow or deep coal seams. What are the similarities and differences between them? Why do these differences exist? What are the different formation mechanisms? Understanding these factors is essential to develop effective mitigation measures in the later stage. However, there is currently limited research on the formation mechanism of this difference. Therefore, this study conducted in-depth research on the formation mechanism of differences through actual measurements and similar model experiments.

2. Study Area and Its Surface Failure Characteristics

2.1. Working Face for Shallow Mining

Working face 22407 is located in Ordos, Inner Mongolia Autonomous Region. The mining depth of the working face is 130 m, with 75 m of bedrock and 55 m of loose layer. The dip angle of the coal seam is 1° , and the size of the working face is 3224 m \times 284 m. The working face is mined by using a comprehensive mechanized mining method, and the roof is managed by using the full caving method. The advancing speed of the working face is 15 m per day. The mined 2-2 coal seam has a simple structure and stable endowment, which belongs to the stable coal seam. The overlying rock formation is dominated by sandstone and interspersed with mudstone and sandy mudstone. The working face is mostly thick siltstone and fine-grained sandstone with good stability. The lithology of the overlying rock layer is medium-hard (Figure 2) [25].

Figure 2. Borehole log of working face 22407.

The ratio of the mining depth to the mining thickness of working face 22407 is small, and surface cracks are fully developed. The cracks can be divided into permanent cracks and dynamic cracks. The permanently stretching crack appears above the boundary of the working face, and the width of the crack increases with the advancement of the working face until it reaches the maximum width (Figure 3).

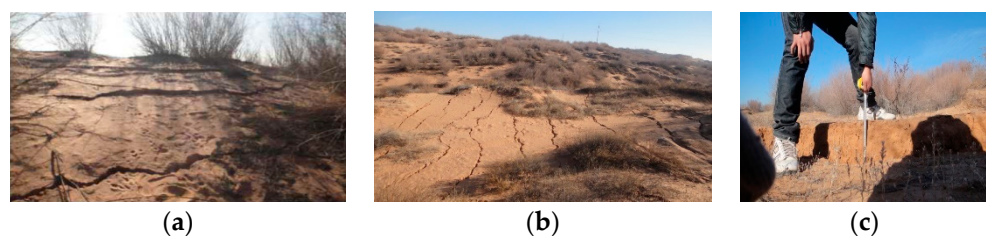


Figure 3. Surface discontinuous subsidence. (a) Permanently stretching crack; (b) Dynamic stretching crack; (c) Stepped crack.

Dynamic cracks appear directly above the goaf and can be subdivided into dynamic stretching cracks and stepped cracks. The width of dynamic cracks first increases with the advance of the working face, then decreases after reaching the maximum value, and finally closes.

2.2. Working Face for Deep Mining

Working face 11071 is located in Yuzhou City, Henan Province. The average dip angle of the coal seam is 4° , the average mining thickness of the coal seam is 4 m, and the average mining depth is 508.5 m. The mining method is full-thickness comprehensive mechanized mining with a strike long wall retreating type, and the advancing speed of the working face is 55 m per month.

The direct roof of working face 11071 consists of sandy mudstone that is dark gray in color, with developed horizontal bedding. The layer can be seen with small white mica fragments and is rich in plant fossil fragments and oriental comb teeth. It has a thickness of about 1.0 m. The main roof is made up of medium-coarse-grained sandstone, also dark gray in color, and is mainly composed of quartz and feldspar with a small amount of argillaceous inclusions. The layer mostly contains muscovite and siderite particles with poor sorting, and the overall thickness is about 30 m. The direct bottom is an interbedding of mudstone and siltstone, with gray siltstone containing a small amount of plant fossil fragments and a large number of muscovite slices. The siltstone and mudstone form a strip with a thickness of about 3.3 m. The old bottom is the interbedding of sandy mudstone or fine-grained sandstone, with developed microwave-like bedding and a thickness of about 13 m. The overlying strata of the working face are medium-hard to soft strata.

During the mining of working face 11,071, the surface subsidence basin occurs (Figure 4a). Obvious cracks appear on the surface road above the mining boundary of the working face (Figure 4b), and they extend forward with the advance of the working face. These cracks are permanent; however, no dynamic cracks are observed on the surface above the working face.

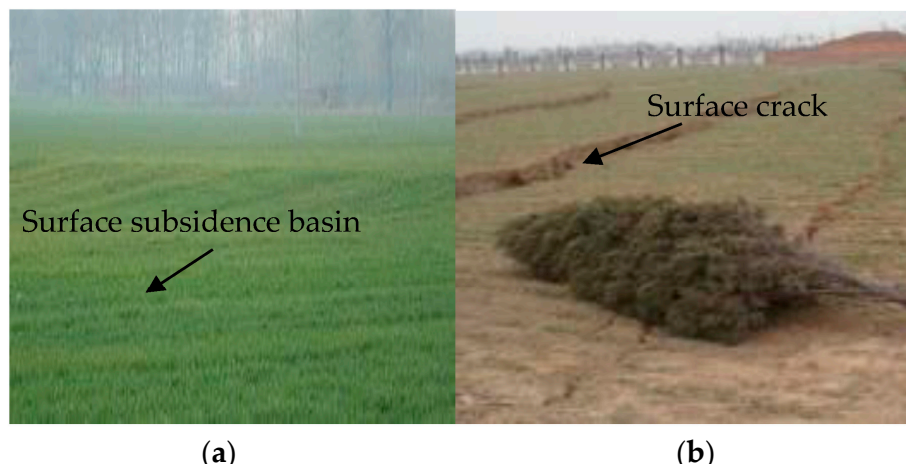


Figure 4. Surface subsidence situation.

3. Methods and Results

This study analyzes the law of overburden movement under shallow and deep mining by using a similar material simulation method to reveal the mechanism of the difference in surface damage between shallow and deep mining.

3.1. Similar Material Simulation in Shallow Mining

3.1.1. Design and Production of Model

The working face 22407 served as the sample for the model test, with a plane model frame measuring 3000 mm × 1600 mm × 250 mm selected. The model experiment design diagram is shown in Figure 5.

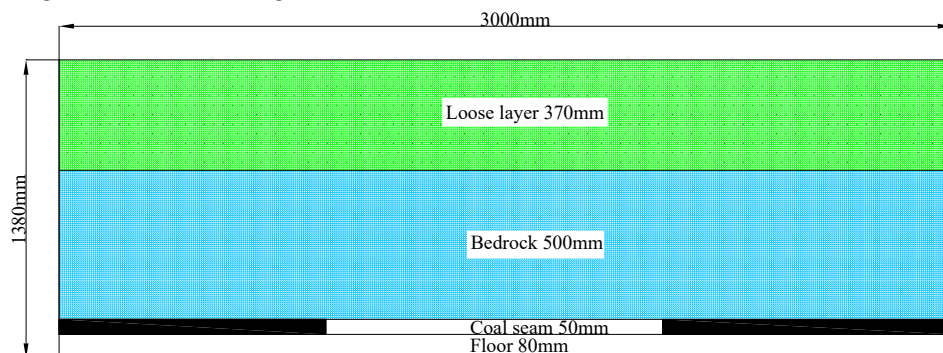


Figure 5. Design diagram of model test.

In accordance with the geological and mining conditions of the simulated working face, 45° was selected as the boundary angle. The geometric dimension relationship between the simulated working face and the model frame was compared and analyzed, and the geometric dimension ratio of 1:150 was finally selected. The unit weight ratio is 0.6, based on the characteristics of overburden and simulated materials. The stress ratio and time ratio can be obtained by using the following formula:

$$\alpha_\sigma = \alpha_{fl} \times \alpha_1 = 0.6 \times (1/150) = 0.004 \quad (1)$$

$$\alpha_t = \sqrt{\alpha_1} = \sqrt{1/150} = 0.082 \quad (2)$$

where: α_σ is the stress ratio; α_{fl} is the unit weight ratio; α_1 is the geometric dimension ratio; and α_t is the time ratio.

In accordance with the experience and the simulated lithology of each rock stratum, the bedrock is mainly composed of sand, with calcium carbonate and gypsum used as cementation auxiliary materials. The loose layer consists mainly of loose sand, supplemented by sawdust. The mica powder is evenly spread as the joint surface between the rock layers after each layer is paved. The material ratio of each layer of rock is shown in Table 1.

Table 1. Proportioning table of model one.

Number	Name	Thickness (cm)	Weight/kg	Material Consumption				
				Sand/kg	Calcium Carbonate/kg	Gypsum/kg	Water/kg	Sawdust/kg
1	Aeolian sand	36.98	301.46	262.01				39.45
2	Sandy mudstone	3.26	36.08	32.07	2.81	1.20	2.16	
3	Siltstone	3.57	39.01	34.14	1.46	3.41	2.34	
4	Medium-grained sandstone	4.32	49.99	39.99	3.00	7.00	3.00	
5	Fine-grained sandstone	3.05	34.03	29.17	1.46	3.40	2.04	

Table 1. Cont.

Number	Name	Thickness (cm)	Weight/kg	Material Consumption				
				Sand/kg	Calcium Carbonate/kg	Gypsum/kg	Water/kg	Sawdust/kg
6	Siltstone	3.25	35.52	31.08	1.33	3.11	2.13	
7	Medium-grained sandstone	9.28	107.38	85.91	6.44	15.03	6.44	
8	Siltstone	1.35	14.75	12.91	0.55	1.29	0.89	
9	Fine-grained sandstone	4.58	51.10	43.80	2.19	5.11	3.07	
10	Fine-grained sandstone	2.43	27.11	23.24	1.16	2.71	1.63	
11	Medium-grained sandstone	2.95	34.14	27.31	2.05	4.78	2.05	
12	Fine-grained sandstone	3.77	42.07	36.06	1.80	4.21	2.52	
13	Sandy mudstone	2.19	24.24	21.54	1.88	0.81	1.45	
14	Medium-grained sandstone	1.89	21.87	17.50	1.31	3.06	1.31	
15	Siltstone	2.23	24.37	21.32	0.91	2.13	1.46	
16	Coal seam	5	42.86	38.57	3.43	0.86	2.57	
17	Siltstone	10	115.71	92.57	6.94	16.20	6.94	

3.1.2. Overburden and Surface Damage Law

The model was dried for one week and then excavated 15 cm at a time. The next stage of excavation could only be conducted after the model's movement became stable. This experiment assumed that the movement of the model rock stratum could reach a stable state 2 h after each excavation. Therefore, the time interval between the two excavations was about 2 h. The method of full height and section excavation at one time was adopted during the simulated excavation.

In the process of gradual excavation, the overburden failure at each stage was as follows (Figure 6).

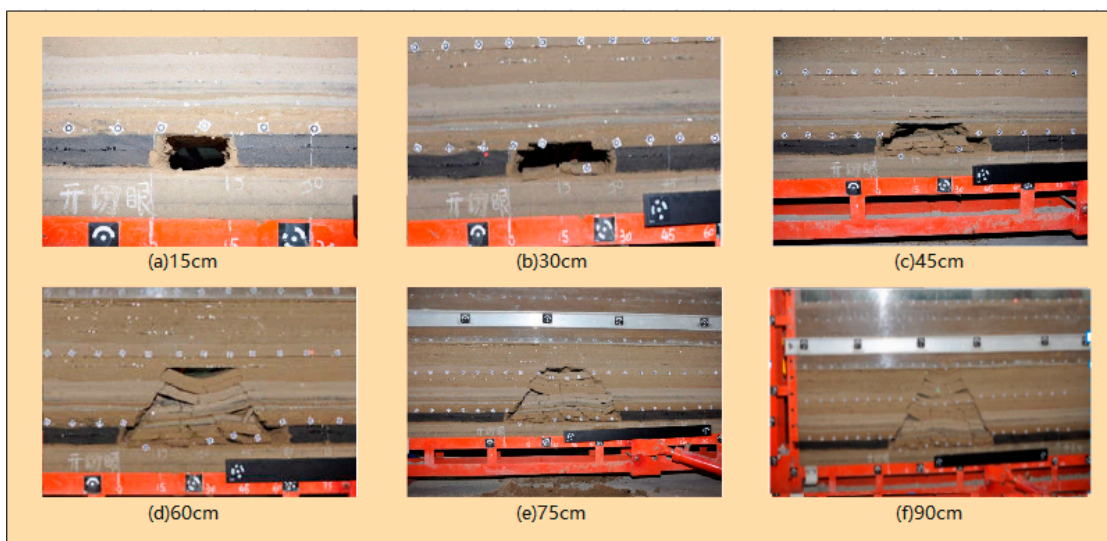


Figure 6. Overburden failure at each stage.

(1) When the working face was excavated to a depth of 15 cm, the roof above the coal seam was not damaged, and no falling phenomenon occurred.

(2) When the working face was excavated to a depth of 30 cm, the false roof above the coal seam was broken. Broken rock blocks accumulated in blocks in the goaf.

(3) When the working face was excavated to a depth of 45 cm, the tensile stress of the direct roof above the coal seam exceeded its tensile strength, and a tensile break occurred in the middle of the direct roof.

(4) When the working face was excavated to a depth of 60 cm, the old roof above the coal seam was broken. With the forward excavation of the working face, the roof of the coal seam continued to collapse, and the collapse height continued to increase, forming an approximate trapezoidal collapse space above the collapsed rock block.

(5) When the working face was excavated to a depth of 90 cm, the overlying bedrock of the coal seam was completely broken. Figure 7a,b show the overburden and surface damage, respectively. The damage to the overlying rock and surface can be described as shown in Figure 7c. The bedrock and loose layer above the goaf were all broken, and the overburden movement in the shallow coal seam mining followed a “two zones” mode, where only caved and fractured zones existed. The overburden was damaged directly up to the surface. Two types of dynamic crack were found above the goaf, which were stepped crack and dynamic stretching crack. The surface above the mining boundary exhibited a permanently stretching crack due to horizontal tension. This condition was consistent with the observed surface damage pattern in shallow mining.

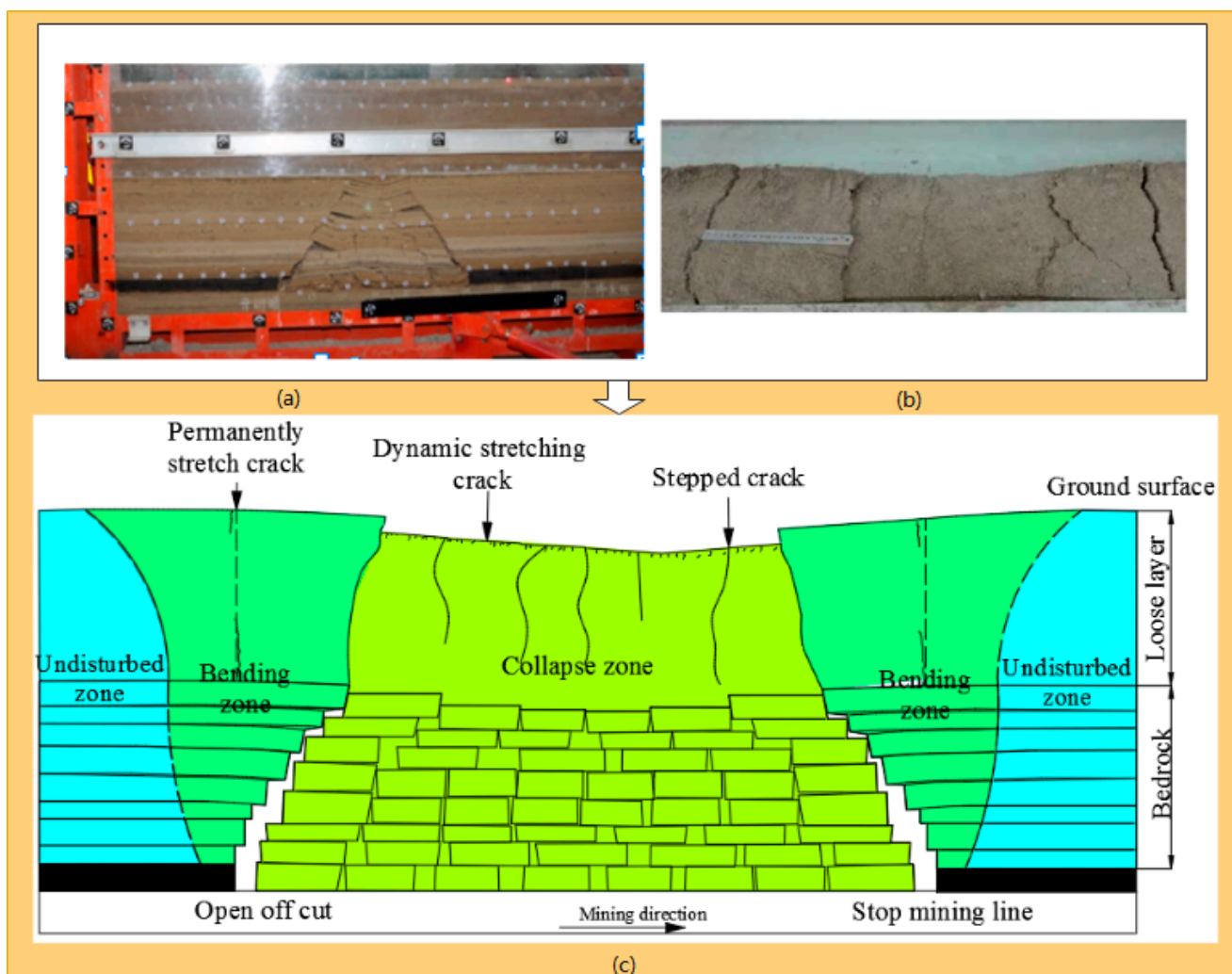


Figure 7. Overburden and surface damage induced by shallow mining. (a) Overburden damage; (b) Surface damage; (c) Schematic.

3.2. Similar Material Simulation in Deep Mining

3.2.1. Design and Production of Model

The working face 11071 was selected for the similar material simulation experiment in deep mining. In combination with the geological and mining conditions and experimental conditions of the mining area, a scale of 1:300 was selected, with a model size of $3.0\text{ m} \times 0.25\text{ m} \times 1.66\text{ m}$. The simulated mining depth was 480.00 m, and the simulated coal thickness was 6 m, as shown in Figure 8.

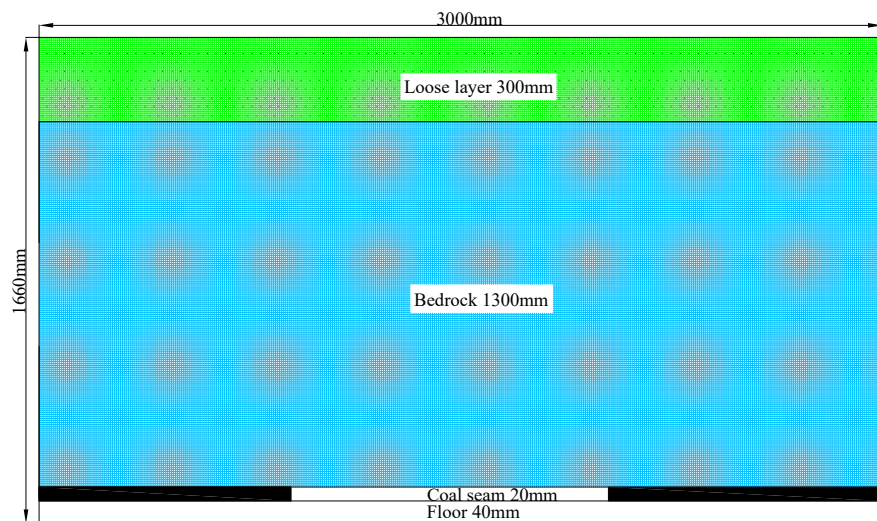


Figure 8. Design diagram of deep mining model test.

On the basis of the geological and mining conditions of the mining area and the available literature, the similarity coefficients selected for the experiment were as follows:

(1) Geometric ratio

$$\alpha_L = L_m / L_p = 1/300 \quad (3)$$

(2) Time ratio

$$\alpha_t = t_m / t_p = \sqrt{\alpha_L} = \sqrt{1/300} = 17.32 \quad (4)$$

(3) Unit weight similarity coefficient

$$\alpha_r = f_l m / f_l p = 0.6 \quad (5)$$

(4) Strength ratio

$$\alpha_\sigma = \frac{\sigma_m}{\sigma_p} = \frac{f_l m \times L_m}{f_l p \times L_p} = \alpha_{f_l} \times \alpha_L = 0.002 \quad (6)$$

The material ratios are shown in Table 2.

Table 2. Material selection and matching for the similar material simulation experiment.

Number	Name	Thickness (cm)	Weight/kg	Material Consumption				
				Sand/kg	Calcium Carbonate/kg	Gypsum/kg	Water/kg	Sodium Borate/g
1	Loose layer	30	375.5	331.8	17.7	25.9	41.6	417.2
2	Medium-grained sandstone	2.79	47.38	40.61	3.38	3.38	5.26	52.64
3	Mudstone	10.84	180.7	161.91	10.08	8.71	20.09	200.75
4	Siltstone	0.93	15.62	13.89	0.87	0.87	1.74	17.36

Table 2. Cont.

Number	Name	Thickness (cm)	Weight/kg	Material Consumption				
				Sand/kg	Calcium Carbonate/kg	Gypsum/kg	Water/kg	Sodium Borate/g
5	Medium-grained sandstone	1.66	28.19	24.16	2.01	2.01	3.13	31.32
6	Mudstone	2.98	49.15	43.27	4.4	1.48	5.47	54.61
7	Siltstone	6.44	108.3	96.28	6.03	6.03	12.03	120.3
8	Medium-grained sandstone	6.24	106.18	91	7.58	7.58	11.8	117.98
9	Siltstone	4.03	67.29	59.8	3.73	3.73	7.48	74.77
10	Sandy mudstone	2.29	37.73	33.01	3.77	0.94	4.19	41.92
11	Siltstone	5.95	99.96	88.81	5.57	5.57	11.09	111.05
12	Medium-grained sandstone	1.72	29.21	25.03	2.09	2.09	3.25	32.45
13	Sandy mudstone	1.74	28.62	25.05	2.86	0.72	3.18	31.81
14	Medium-grained sandstone	6.79	115	98.6	8.23	8.23	12.78	127.87
15	Siltstone	2.3	37.16	33.03	2.06	2.06	4.13	41.29
16	Medium-grained sandstone	5.3	89.88	77.05	6.42	6.42	9.99	99.87
17	Sandy mudstone	40.72	677.3	594.46	54.89	27.85	75.27	752.58
18	Siltstone	4.57	76.85	67.4	4.72	4.72	8.54	85.39
19	Medium-grained sandstone	2.56	43.47	37.26	3.1	3.1	4.83	48.3
20	Sandy mudstone	7.7	127.01	111.11	12.71	3.18	14.12	141.11
21	Siltstone	2.07	34.6	30.75	1.92	1.92	3.84	38.44
22	Medium-grained sandstone	10.38	181.6	155.63	12.98	12.98	20.16	201.76
23	Coal seam	2	23.36	20.77	1.82	0.78	2.6	25.96
24	Siltstone	1.6	14.28	12.7	0.79	0.79	1.59	15.87
25	Sandy mudstone	2.4	39.48	34.54	3.94	0.98	4.38	43.86

3.2.2. Overburden and Surface Damage Law

The model was dried for one week and then excavated for 10 cm at a time. The next stage of excavation could only be conducted after the model's movement became stable. This experiment assumed that the movement of the rock stratum could reach a stable state 2 h after each excavation. Therefore, the time interval between the two excavations was about 2 h.

The method of full height at one time was adopted during the simulated excavation. In the process of gradual excavation, the overburden failure at each stage was as follows (Figure 9).

As the excavation proceeded, the direct roof continued to collapse, until it stabilized at a height of 200 cm. The fractured zone extended 116 cm from the coal seam, and the maximum height of the caved zone was 3.2 cm, as shown in Figure 10. Figure 10a shows the overburden damage. Figure 10b illustrates the damage of the overlying rock. The overburden movement in deep coal seam mining was characterized by a "three zones" mode, with the caved zone, fractured zone, and sagging zone existing simultaneously.

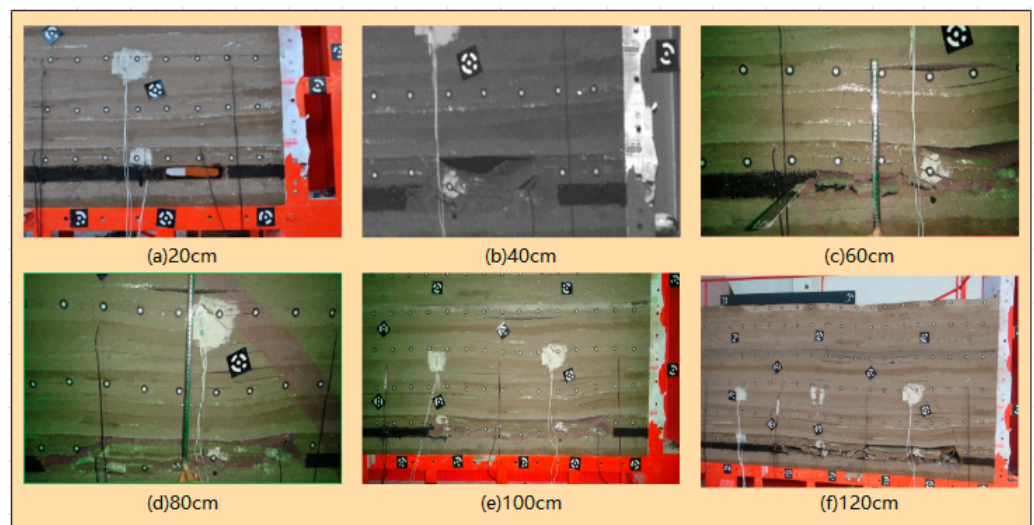


Figure 9. Overburden failure induced by deep mining at each stage.

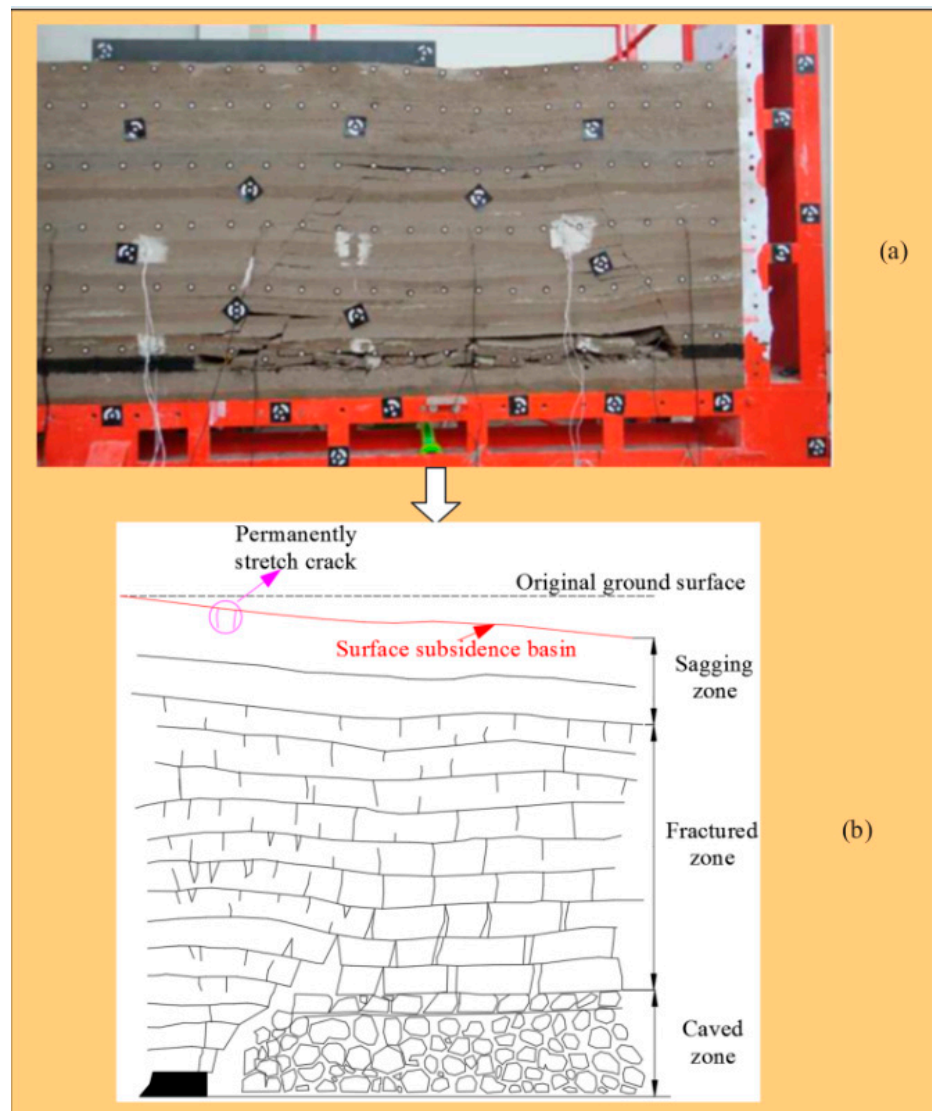


Figure 10. Overburden damage induced by deep mining. (a) Overburden damage; (b) Schematic.

Permanently stretched tensile cracks appeared on the surface above the mining boundary due to horizontal tension, and the surface subsidence occurred in the continuous form of a surface subsidence basin above the goaf. This condition was consistent with the observed surface damage law of deep mining.

4. Discussion

4.1. Formation Mechanism of Permanently Stretch Cracks

Overlying strata move toward the goaf after an underground coal seam is mined. The strata above the mined coal seam are broken layer by layer, and the broken rock blocks fill the goaf. In the vicinity of the mining boundary, the broken rock strata are in the form of cantilever beams. From the mined coal seam upward, the length of the overhanging rock block increases, as shown in Figure 11a. The overhanging rock block and its overlying loose layer can be simplified as wedge block B in Figure 11b. Before mining, wedge block B is subject to the thrust of its left rock stratum, the thrust of its right rock stratum, and the supporting force of the underlying rock stratum. The balance of mechanics is maintained under the combined action of these forces.

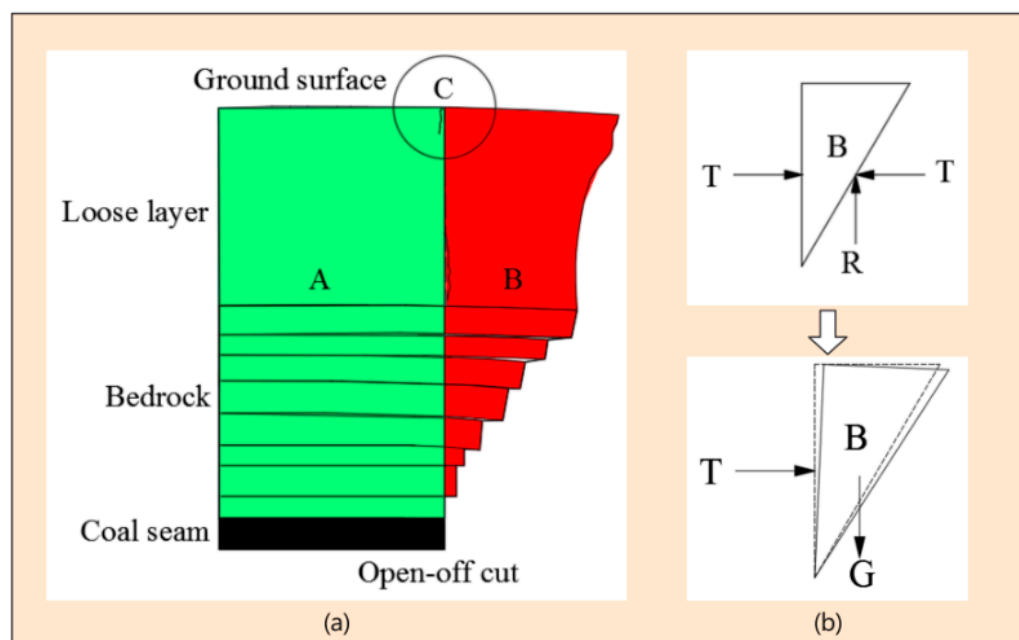


Figure 11. Formation mechanism of permanently stretched crack. (a) Wedge; (b) Force analysis.

After mining, the thrust T and supporting force R of the right and underlying strata on B decrease because of the movement of the right and lower pumice strata toward the goaf, resulting in rock block B tilting to the lower right under the combined action of the thrust of the left rock strata on it and its own self-weight force G . Thus, B and A rock blocks stretch at surface point C , and tensile cracks appear. Rock block B cannot be restored after it tilts, so the crack will remain permanent after it appears, which is called a permanently stretched crack.

The above processes occur in shallow and deep coal seams, making permanently stretched cracks easily occur on the surface above the mining boundary.

4.2. Formation Mechanism of Dynamic Crack

The impact of underground mining on the ground surface is mainly reflected in two aspects: the subsidence range and maximum subsidence value. According to the mining subsidence theory, when the working face is advanced to a certain distance, the maximum subsidence value of the surface will reach the maximum, and it will not increase in the

future. To effectively represent the subsidence effects of each mining stage, the concept of the mining degree was introduced. The degree of mining is calculated as follows:

$$D = \frac{L}{H} \quad (7)$$

where D is the mining degree, L is the mining width, and H is the mining depth.

When the mining degree D reaches 1.2–1.4, the surface subsidence value reaches the maximum. Subsequently, the working face is excavated, and the maximum subsidence value of the surface will no longer increase, but only increase the subsidence range. According to the results of the two similar models, the change of the fracture height of the rock formation with the mining degree is shown in Figure 12.

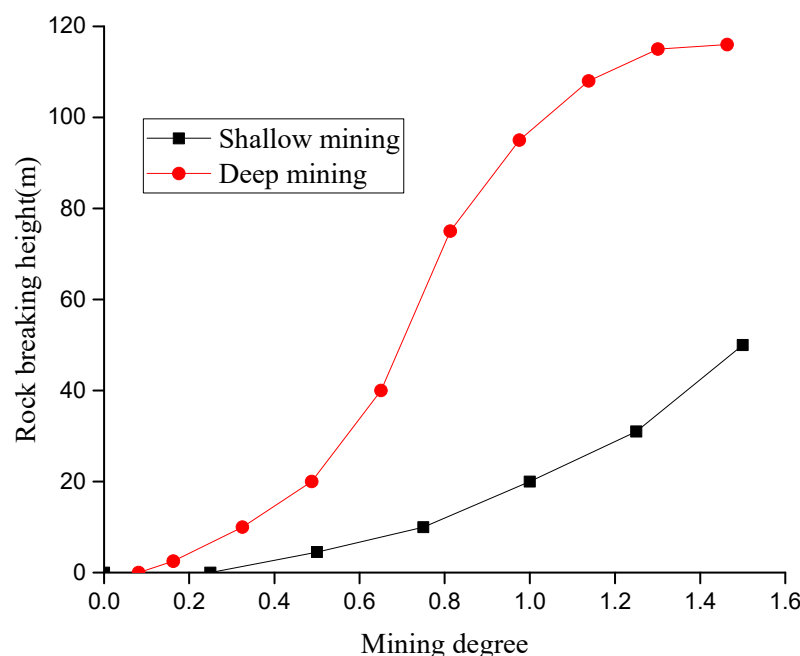


Figure 12. Development law of rock damage height.

Under the condition of deep burial, the damage height of rock strata in the model test increases with the mining degree, showing an S-shaped development trend.

(1) The inflection point of the rock damage height development curve is about 0.6–0.8. Before the inflection point, with the increase of the mining degree, the overburden failure height increased rapidly, and the increase rate gradually increased.

(2) At the inflection point (mining degree 0.6–0.8), the overburden failure height is still increasing, and the increase rate is the maximum.

(3) After exceeding the inflection point, with the increase of mining degree, the overburden failure height still continues to increase, but the increase rate gradually decreases.

(4) When the mining degree reaches 1.2–1.4, the overburden failure height reaches the maximum value. The damage height of overlying rock does not increase further during subsequent mining.

In accordance with the theory of “three zones,” the rock strata above the maximum damage height up to the surface form the sagging zone, where the overlying rock moves continuously without experiencing discontinuous deformation, such as cracks. Therefore, no dynamic crack occurs on the surface above the working face under the condition of deep mining. The overburden movement in deep coal seam mining is “three zones” mode.

However, the development law of rock damage height in shallow coal mining is obviously different from that in deep mining. The damage height of rock strata in shallow thick coal seam mining increases exponentially with the mining degree.

(1) With the increase of mining degree, the overburden failure height increases rapidly, and the increase rate gradually increases.

(2) The larger the mining degree is, the larger the rock damage height caused by the same, until the damage extends to the bedrock surface.

In this case, the overburden is broken directly to the surface of the bedrock, and there is no sagging zone in the overburden, only a collapse zone and a fracture zone, that is, the overburden movement in shallow coal seam mining is in a “two zones” mode.

According to literature [25], the rock strata migrate in the form of bench rock beams under shallow mining conditions. The stability of the step rock beam mainly depends on the relationship between the friction and shear force at the overlap of rock blocks. If the shear force is greater than the friction force, then the step rock beam structure will slide and lose stability.

Rock block N_2 falls completely on the collapsed rocks and presents a compacted state, so R_2 is equal to P_2 .

According to the moment equilibrium equations $\sum M_A = 0$ and $\sum M_B = 0$, Equations (8) and (9) can be derived.

$$Q_A + Q_B = P_1 \quad (8)$$

$$T = \frac{IP_1}{2(h - a - w)} = \frac{P_1}{i - 2 \sin \theta_{\max} + \sin \theta} \quad (9)$$

where i is the rock fragmental size, $i = l/h$.

The shear force of point B can be calculated in accordance with Equation (10) as follows:

$$Q_B = T \sin \theta_2 \quad (10)$$

θ_2 is very small; hence, Q_B can be ignored, and $Q_A = P_1$ can be concluded.

According to literature [25], the relationship between the friction force and the shear force at the overlap of the broken rock block of the bench rock beam under the mining of shallow coal seams is as follows:

$$T \tan \varphi = \frac{P_1}{i - 2 \sin \theta_{\max} + \sin \theta} \tan \varphi < P_1 = Q_A \quad (11)$$

where T is the horizontal thrust. Q_A is the shear forces of points A. P_1 is the suffered load of the rock N_1 . i is the rock fragmental size. θ is the rock rotation angle.

In accordance with the above formula, the shear force is greater than the friction force, and the joint of the broken rock block is prone to slip and instability. The sliding and instability of the roof cause the overlying strata to cut off and create step subsidence.

The loose layer relative to the bedrock is similar to a random medium, and its antideformation ability is mostly negligible when faced with the step subsidence transmitted from the bedrock. Thus, the step subsidence is transmitted to the ground surface, which is represented by a stepped crack.

As shown in Figure 13b, rock blocks N_1 and N_2 are broken during mining. N_2 is subject to sliding instability, and step subsidence occurs between the N_1 and N_2 rock blocks. As the working face continues to advance, sliding instability also occurs between N_1 and the left rock block. The step subsidence between the N_1 and N_2 rock blocks disappears. Similarly, the stepped crack and dynamic tensile crack on the surface above the working face appear first and then disappear, with an automatic closing function.

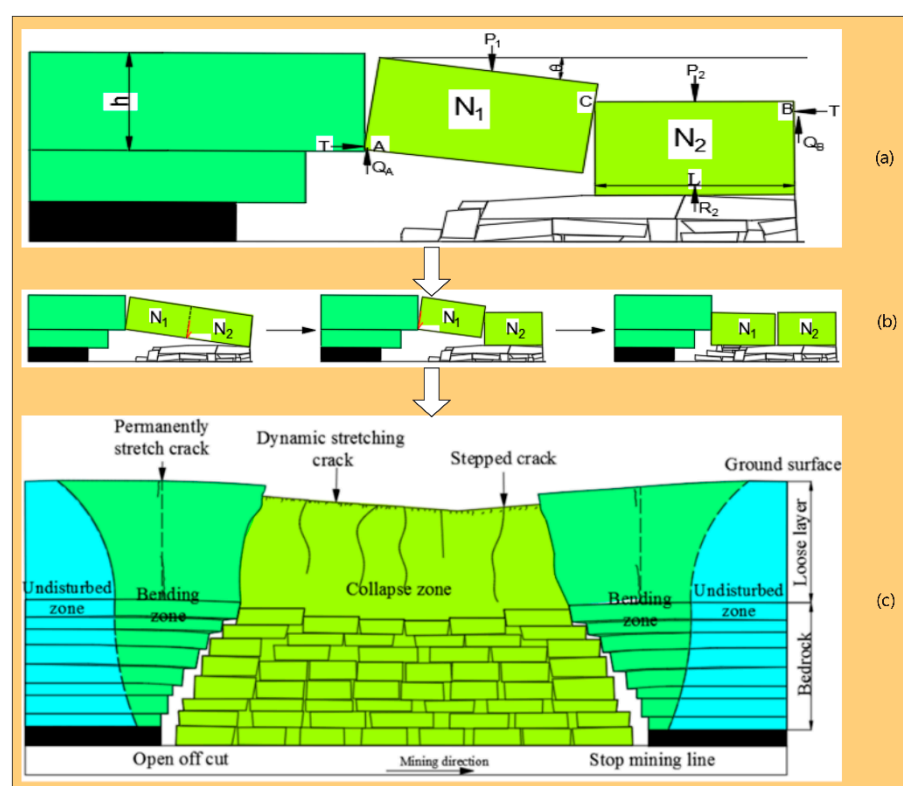


Figure 13. Formation mechanism of dynamic crack. (a) Force analysis; (b) Process of rock damage; (c) Schematic of final damage.

5. Conclusions

Understanding the formation mechanism of surface damage differences in deep and shallow mining is vital for disaster prevention and environmental protection. In this work, the formation mechanism was systematically analyzed by combining a similarity simulation experiment and geo-mining conditions of the relevant working face. The conclusions are summarized as follows:

- (1) Under the condition of deep mining, the damage height of rock strata increases with the mining degree, showing a S-shaped development trend. However, the damage height of rock strata has an exponential development trend, with the mining degree under the condition of shallow mining.
- (2) Under the mining of shallow coal seams, permanently stretched cracks above the mining boundary and dynamic cracks above the goaf on the surface are found. However, only permanently stretched cracks are observed on the surface above the mining boundary under the mining of deep coal seams.
- (3) The rock strata inside the mining boundary develop into a wedge-shaped block due to the mining of underground coal seams. It inclines under the action of the horizontal thrust of nearby rock strata and self-gravity, resulting in a permanently stretched crack above the mining boundary.
- (4) The overburden movement in deep coal seam mining is “three zones” mode. The overburden movement in shallow coal seam mining is in a “two zones” mode. The overburden strata slide and become unstable in the form of a bench rock beam, resulting in stepped cracks and dynamic stretching cracks on the surface above the goaf.

Author Contributions: Conceptualization, W.Y.; methodology, W.Y.; software, J.G.; validation, S.Y.; formal analysis, W.Y.; investigation, S.Y.; resources, S.Y.; data curation, W.Y.; writing—original draft preparation, W.Y.; writing—review and editing, S.Y.; visualization, S.Y.; supervision, J.G.; project administration, W.Y.; funding acquisition, S.Y. All authors have read and agreed to the published version of the manuscript.

Funding: This research was funded by the Open Fund of the State Key Laboratory of Water Resource Protection and Utilization in Coal Mining grant number (WPUKFJJ2019-17), the National Natural Science Foundation of China grant number (42207534, U21A20108), the Youth Backbone Teacher Support Program of Henan Polytechnic University (2019XQG-07), and the Doctoral Fund Program of Henan Polytechnic University (B2017-07, B2019-03).

Institutional Review Board Statement: Not applicable.

Informed Consent Statement: Not applicable.

Data Availability Statement: Not applicable.

Conflicts of Interest: The authors declare no conflict of interest.

References

- Yan, W.; Chen, J.; Tan, Y.; He, R.; Yan, S. Surface dynamic damage prediction model of horizontal coal seam based on the idea of wave lossless propagation. *Int. J. Environ. Res. Public Health.* **2022**, *19*, 6862. [[CrossRef](#)]
- Vervoort, A. The Time Duration of the Effects of Total Extraction Mining Methods on Surface Movement. *Energies* **2020**, *13*, 4107. [[CrossRef](#)]
- Ju, J.; Xu, J. Surface stepped subsidence related to top-coal caving longwall mining of extremely thick coal seam under shallow cover. *Int. J. Rock Mech. Min. Sci.* **2015**, *78*, 27–35. [[CrossRef](#)]
- Orwat, J. Causes analysis of occurrence of the terrain surface discontinuous deformations of a linear type. *J. Phys.* **2020**, *1426*, 012016. [[CrossRef](#)]
- Strzałkowski, P.; Ścigała, R.; Szafulera, K.; Tomiczek, K. *Forecasting of Discontinuous Deformations of Surface Type on the Mining and Post-Mining Areas*; Publishing House of Silesian University of Technology: Gliwice, Poland, 2020; p. 127.
- Vervoort, A. Impact of the closure of a coal district on the environmental issue of long-term surface movements. *AIMS Geosci.* **2022**, *8*, 326–345. [[CrossRef](#)]
- Peng, S. *Coal Mine Ground Control*, 3rd ed.; West Virginia University: Morgantown, WV, USA, 2008.
- Strzałkowski, P.; Ścigała, R.; Szafulera, K.; Kołodziej, K. Surface Deformations Resulting from Abandoned Mining Excavations. *Energies* **2021**, *14*, 2495. [[CrossRef](#)]
- Strzałkowski, P. Predicting mining areas deformations under the condition of high strength and depth of cover. *Energies* **2022**, *15*, 4627. [[CrossRef](#)]
- Guo, J.; Li, Q.; Xie, H. Monitoring of vegetation disturbance and restoration at the dumping sites of the baorixile open-pit mine based on the LandTrendr algorithm. *Int. J. Environ. Res. Public Health.* **2022**, *19*, 9066. [[CrossRef](#)]
- Radutu, A.; Vlad-Sandru, M.-I. Review on the Use of Satellite-Based Radar Interferometry for Monitoring Mining Subsidence in Urban Areas and Demographic Indicators Assessment. *Min. Rev./Rev. Minelor.* **2023**, *29*, 42–62. [[CrossRef](#)]
- Rezaei, M.; Hossaini, M.F.; Majdi, A. A time-independent energy model to determine the height of destressed zone above the mined panel in longwall coal mining. *Tunn. Undergr. Space Technol.* **2015**, *47*, 81–92. [[CrossRef](#)]
- Salmi, E.F.; Nazem, M.; Karakus, M. Numerical analysis of a large landslide induced by coal mining subsidence. *Eng. Geol.* **2017**, *217*, 141–152. [[CrossRef](#)]
- Bai, E.; Guo, W.; Tan, Y. Negative externalities of high-intensity mining and disaster prevention technology in China. *Bull. Eng. Geol. Environ.* **2019**, *78*, 5219–5235. [[CrossRef](#)]
- Tajdu’s, K.; Sroka, A.; Misa, R.; Hager, S.; Rusek, J.; Dudek, M.; Wollnik, F. Analysis of Mining-induced delayed surface subsidence. *Minerals* **2021**, *11*, 1187. [[CrossRef](#)]
- Modeste, G.; Doubre, C.; Masson, F. Time evolution of mining-related residual subsidence monitored over a 24-year period using InSAR in southern Alsace, France. *Int. J. Appl. Earth Obs. Geoinf.* **2021**, *102*, 102392. [[CrossRef](#)]
- Declercq, P.-Y.; Dusar, M.; Pirard, E.; Verbeurg, J.; Choopani, A.; Devleeschouwer, X. Post Mining Ground Deformations Transition Related to Coal Mines Closure in the Campine Coal Basin, Belgium, Evidenced by Three Decades of MT-InSAR Data. *Remote Sens.* **2023**, *15*, 725. [[CrossRef](#)]
- Li, P.; Zhu, X.; Ding, X.; Zhang, T. An Experimental Study of Industrial Site and Shaft Pillar Mining at Jinggezhuang Coal Mine. *Appl. Sci.* **2023**, *13*, 2340. [[CrossRef](#)]
- Wang, Z.; Li, W.; Wang, Q. Monitoring the dynamic response of the overlying rock-soil composite structure to underground mining using BOTDR and FBG sensing technologies. *Rock Mech. Rock Eng.* **2021**, *54*, 5095–5116. [[CrossRef](#)]
- Dong, L.; Zhu, H.; Yan, F.; Bi, S. Risk field of rock instability using microseismic monitoring data in deep mining. *Sensors* **2023**, *23*, 1300. [[CrossRef](#)] [[PubMed](#)]
- Dudek, M.; Tajdu’s, K. FEM for prediction of surface deformations induced by flooding of steeply inclined mining seams. *Geomech. Energy Environ.* **2021**, *28*, 100254. [[CrossRef](#)]
- Bo, H.; Li, Y.; Tan, X.; Dong, Z.; Zheng, G.; Wang, Q.; Yu, K. Estimation of Ground Subsidence Deformation Induced by Underground Coal Mining with GNSS-IR. *Remote Sens.* **2022**, *15*, 96. [[CrossRef](#)]
- Fan, K.; Li, W.; Wang, Q. Formation mechanism and prediction method of water inrush from separated layers within coal seam mining: A case study in the Shilawusu mining area China. *Eng. Fail. Anal.* **2019**, *103*, 158–172. [[CrossRef](#)]

24. Yan, W.; Chen, J.; Yan, Y. A new model for predicting surface mining subsidence: The improved lognormal function model. *Geosci. J.* **2019**, *23*, 165–174. [[CrossRef](#)]
25. Yan, W.; Dai, H.; Chen, J. Surface crack and sand inrush disaster induced by high-strength mining: Example from the Shendong coal field, China. *Geosci. J.* **2018**, *22*, 347–357. [[CrossRef](#)]

Disclaimer/Publisher’s Note: The statements, opinions and data contained in all publications are solely those of the individual author(s) and contributor(s) and not of MDPI and/or the editor(s). MDPI and/or the editor(s) disclaim responsibility for any injury to people or property resulting from any ideas, methods, instructions or products referred to in the content.